Geosci. Model Dev., 19, 11405–11418, 2026
https://doi.org/10.5194/gmd-19-11405-2026
© Author(s) 2026. This work is distributed under
the Creative Commons Attribution 4.0 License.

Geoscientific Model Development
Open Access
EGU

Kinetic partitioning with effective mass accommodation for secondary organic aerosol simulations in chemical transport modeling

Regina Luu[1], **Meredith Schervish**[1,a], **Samuel E. O'Donnell**[2], **Jeffrey R. Pierce**[2], **and Manabu Shiraiwa**[1]

[1]Department of Chemistry, University of California, Irvine, CA, 92617, USA
[2]Department of Atmospheric Science, Colorado State University, Fort Collins, CO, 80521, USA
[a]now at: Department of Veterinary Physiology and Pharmacology, Texas A&M University, College Station, TX, 77843, USA

Correspondence: Manabu Shiraiwa (m.shiraiwa@uci.edu)

Received: 6 August 2026 – Discussion started: 27 August 2026
Revised: 3 November 2026 – Accepted: 18 November 2026 – Published: 27 November 2026

Abstract. Secondary organic aerosols (SOA) can adopt liquid, amorphous semi-solid, or glassy solid states in the atmosphere. Previous model simulations have revealed that SOA adopt semisolid or glassy solid phase states over dry regions and in the upper troposphere. A highly viscous phase state in SOA particles can cause kinetic limitations in SOA partitioning, challenging traditional SOA treatments with equilibrium partitioning in chemical transport modeling. In this study, we develop a method to simulate kinetic partitioning of SOA accounting for the impacts of SOA phase state by utilizing effective mass accommodation coefficient (α_{eff}). This method effectively accounts for the effects of gas-phase diffusion, represented by the condensation sink, as well as particle phase state and the associated kinetic limitations on partitioning. We initially test this method in box modeling to calculate equilibration timescales of SOA partitioning for a wide parameter space for bulk diffusivity, volatility, and total aerosol mass loading. Comparison with the chemical timestep of 20 min in GEOS-Chem reveals that equilibrium partitioning is still applicable for particles with bulk diffusivity $> 10^{-15}$ cm^2 s^{-1}, whereas kinetic partitioning is required for partitioning of semi-and low-volatile compounds into highly viscous particles. To reduce computational burden, we developed analytical equations with gas-particle mass transfer coefficients effectively accounting for gas and bulk diffusion limitations. The application of the new α_{eff} kinetic partitioning scheme into GEOS-Chem predicts lower SOA mass over drylands (e.g., Western US) in the boundary layer due to kinetically limited growth of viscous SOA particles, whereas SOA mass can be described well with equilibrium partitioning in most other areas at the surface and at 850 hPa. In the upper troposphere at 500 hPa, the α_{eff}-kinetic scheme predicts up to 50 % higher SOA mass as evaporation is suppressed for glassy particles. The developed method is easily applicable, improving description and treatments of SOA in chemical transport models.

1 Introduction

Secondary organic aerosols (SOA) are ubiquitous and represent a major fraction of the submicron particulate matter in the troposphere, playing a central role in aerosol effects on climate, air quality, and public health (Jimenez et al., 2009; Pöschl and Shiraiwa, 2015; Shrivastava et al., 2017). Unlike primary organic aerosols which are directly emitted into the atmosphere, SOA are mainly formed in the atmosphere from the oxidation of biogenic or anthropogenic volatile organic compounds (VOCs) into lower-volatility products that may nucleate or condense onto pre-existing particles (Hallquist et al., 2009; Kirkby et al., 2023; Kroll and Seinfeld, 2008). Other pathways of SOA formation include aqueous/heterogeneous chemistry and volatilization and subsequent oxidation of gases from primary organic aerosols (Robinson et al., 2007; Ziemann and Atkinson, 2012). SOA formation has been extensively studied in laboratory experiments, but there is still a significant gap between ambient measurements and model simulations of SOA concentrations and properties by

chemical transport models (CTMs) (Hallquist et al., 2009; Hodzic et al., 2016; Tsigaridis et al., 2014).

An important physical property of SOA particles is the particle phase state which can vary from liquid (characterized by dynamic viscosity $\eta < 10^2$ Pa s), semisolid ($10^2 < \eta \leq 10^{12}$ Pa s), to glassy solid states ($\eta > 10^{12}$ Pa s) depending on the chemical composition, temperature, and relative humidity (Koop et al., 2011; Reid et al., 2018; Virtanen et al., 2010). Traditionally, SOA particles are assumed implicitly to be liquid-like in CTMs (Chung and Seinfeld, 2002; Pye and Seinfeld, 2010). The assumption holds that the gas-particle equilibration timescale is rapid in comparison to other atmospheric processes implying that SOA particles achieve instantaneous equilibrium partitioning between the gas and particle phases (Pankow, 2003). However, there has been mounting evidence of laboratory measurements and ambient observations showing that SOA can exist in glassy solid or amorphous semisolid states as influenced by chemical composition and ambient conditions (Jensen et al., 2025; O'Brien et al., 2014; Saukko et al., 2012; Vaden et al., 2011; Virtanen et al., 2010). A highly viscous phase state can lead to prolonged equilibration timescales of SOA partitioning, depending on volatility of species and particle mass loadings (Li and Shiraiwa, 2019; Schervish et al., 2024). We have developed methods to predict SOA phase state and viscosity (DeRieux et al., 2018; Li et al., 2020; Shiraiwa et al., 2017); their applications in CTMs suggest that SOA particles should adopt a viscous phase state over drylands and in the free troposphere (Luu et al., 2025; Schmedding et al., 2020; Shiraiwa et al., 2017; Zhang et al., 2024). While there are a few studies explicitly resolving kinetic SOA partitioning (He et al., 2025; Shrivastava et al., 2024), the major limitation in most SOA phase state modeling studies is the phase state prediction being applied as offline and post-processing calculations.

Implementing kinetic partitioning with explicit consideration of the effect of SOA phase state is essential in CTMs to improve SOA budgets and thereby aerosol impacts on air quality, climate, and public health. Process-level microphysics models such as the kinetic multi-layer model of gas-particle interactions in aerosols and clouds (KM-GAP) can resolve kinetic limitations imparted by semi-solid or glassy solid phase states, but applying the same methodology to a CTM would drastically increase computational costs. Therefore, in this work, we develop a model scheme for the partitioning of organic compounds that is modulated by online calculations of SOA phase state by utilizing an effective mass accommodation coefficient (Shiraiwa and Pöschl, 2021). We investigate the influence of particle phase state, volatility, and total organic aerosol concentration on gas-particle partitioning of organic compounds in SOA. Then, we implement our partitioning scheme into the global CTM, GEOS-Chem, to evaluate the impacts of SOA phase state on SOA budgets.

2 Methods

2.1 Validation of partitioning method with a box model

Based on absorptive partitioning theory (Pankow, 1994), the mass transfer rates between gas and particle phases can be expressed for gas- (C^g) and particle-phase (C^p) mass concentrations (in $\mu g\,m^{-3}$) of semi-volatile compounds with the following ordinary differential equations (Shiraiwa and Pöschl, 2021; Trump et al., 2014):

$$\frac{dC^g}{dt} = -k_{gp}\left(C^g - \frac{C^p}{C_{OA}}C^0\right) \quad (1)$$

$$\frac{dC^p}{dt} = k_{gp}\left(C^g - \frac{C^p}{C_{OA}}C^0\right) \quad (2)$$

Partitioning is also dependent on the ratio of particle-phase concentration, C^p, and C_{OA} ($\mu g\,m^{-3}$), the total organic aerosol concentration. C^0 ($\mu g\,m^{-3}$) is the temperature-dependent equilibrium vapor concentration and is described via the Clausius-Clapeyron relation:

$$C^0(T) = C^0(298\,K)\exp\left(\frac{\Delta H_{vap}}{R}\left(\frac{1}{298\,K} - \frac{1}{T}\right)\right) \quad (3)$$

where R is the molar gas constant in $J\,mol^{-1}\,K^{-1}$ and T refers to the ambient temperature in K. Species with a low volatility tend to have a higher enthalpy of vaporization, ΔH_{vap} ($kJ\,mol^{-1}$), as described by the semi-empirical parameterization (Stolzenburg et al., 2018, 2022):

$$\Delta H_{vap} = -5.7 \times \log_{10} C^0(298\,K) + 129 \quad (4)$$

k_{gp} (s^{-1}) is the first-order gas-particle mass transfer coefficient or the condensation sink, which we approximate by assuming a monodisperse aerosol population:

$$k_{gp}(\beta) = 2\pi D_g D_p N_p \beta \quad (5)$$

$$\beta(Kn, \alpha_{eff}) = \frac{0.75\alpha_{eff}(1+Kn)}{Kn^2 + Kn + 0.283Kn\alpha_{eff} + 0.75\alpha_{eff}} \quad (6)$$

Where D_g ($cm^2\,s^{-1}$) is the gas-phase diffusivity and D_p (cm) is the particle diameter. The term β is the Fuchs-Sutugin correction factor for gas diffusion in the transition regime, which is a function of the Knudsen number (Kn) and the effective mass accommodation coefficient (α_{eff}). Kn is the ratio of the mean free path in the gas phase (λ) as calculated using the mean thermal velocity (ω), and D_p: $Kn = 2\lambda/D_p = 6D_g/(\omega D_p)$ (Pöschl et al., 2007). We assume a monodisperse particle population initialized at $D_p = 100$ nm with particle growth/loss considered only through condensation/evaporation as the number concentration is held constant while C_{OA} may vary.

α_{eff} describes the probability of a gas molecule colliding with a particle surface to enter the condensed phase, considering potential kinetic limitation of bulk diffusion in the

particle phase as described as follows (Shiraiwa and Pöschl, 2021) (see also Fig. S1a in the Supplement):

$$\alpha_{\text{eff}} = \alpha_{\text{s}} \frac{1}{1 + \frac{\alpha_{\text{s}} \omega C^0}{4 D_{\text{b}} \rho_{\text{p}}} \frac{D_{\text{p}}}{10} \times 10^{-12}} \tag{7}$$

where α_{s} is the surface accommodation coefficient, which is assumed to be 1 (Julin et al., 2014), and ρ_{p} (g cm^{-3}) is the particle density which is assumed to be 1.4 (Kuwata et al., 2012). Note that most studies assume certain fixed values for mass accommodation coefficient (often 1, 0.5, or 0.1) without considering the effect of particle phase state. α_{eff} provides an efficient way of accounting for the influence of species volatility and bulk diffusivity, D_{b} ($\text{cm}^2\,\text{s}^{-1}$) on SOA partitioning (Shiraiwa and Pöschl, 2021). The conversion factor 10^{-12} allows volatility to be inserted in the commonly used $\mu\text{g m}^{-3}$ units. The application of α_{eff} in traditional mass transfer equations yielded consistent simulation results with a kinetic multilayer model (KM-GAP) and two-film model (MOSAIC) (Zaveri et al., 2014) and α_{eff} successfully explained experimentally measured accommodation coefficient in SOA partitioning (Liu et al., 2019; Shiraiwa and Pöschl, 2021).

The stiff ODE system of Eqs. (1) and (2) is solved using the Livermore Solver for Ordinary Differential Equations (DLSODE) in double precision (Hindmarsh, 1983). The use of an ODE solver can be computationally expensive especially when implemented in a CTM; therefore, we also treat Eq. (1) with an exponential approximation accompanied with the assumption that the equilibrium concentration is known a priori. The derivation of this approximation is as follows: at equilibrium, the net mass transfer rate between the gas and particle phase is zero.

$$\frac{\text{d}C^{\text{g}}}{\text{d}t} = 0 \tag{8}$$

Substituting Eq. (1) into Eq. (9) gives the following equation knowing that the condensation sink cannot be zero.

$$\frac{C^{\text{p}}}{C_{\text{OA}}} C^0 = C^{\text{g}}_{\text{eq}} \tag{9}$$

At equilibrium, the gas-phase concentration would be the product of the particle-phase mass fraction of a species and its volatility. Substitution of Eq. (10) into Eq. (1) gives:

$$\frac{\text{d}C^{\text{g}}}{\text{d}t} = -k_{\text{gp}} \left(C^{\text{g}} - C^{\text{g}}_{\text{eq}} \right) \tag{10}$$

Equation (11) can be solved analytically with integration by separation of variables to obtain the following analytical solution of the gas-phase concentration at time, t, when initial and equilibrium concentrations are known as well as the condensation sink of that species.

$$C^{\text{g}}(t) = C^{\text{g}}_0 - \left(C^{\text{g}}_0 - C^{\text{g}}_{\text{eq}} \right) \left(1 - e^{-k_{\text{gp}} t} \right) \tag{11}$$

We conducted model simulations of SOA partitioning using a standalone zero-dimensional box model to calculate and compare two timescales of SOA partitioning, equilibration and mixing timescales, under various environmental conditions and mass loadings. The e-folding timescale to achieve gas-particle equilibrium or otherwise known as the equilibration timescale, τ_{eq} is calculated for the first time instance (t) in which the following inequality is satisfied (Li and Shiraiwa, 2019):

$$\frac{\left| C_{\text{p}}(t) - C_{\text{p.eq}} \right|}{\left| C_{\text{p,0}} - C_{\text{p.eq}} \right|} < \frac{1}{e} \tag{12}$$

$C_{\text{p,0}}$ and $C_{\text{p,eq}}$ refer to the initial and equilibrium mass concentration of a diffusing compound in the particle phase, respectively. τ_{eq} of a partitioning species also corresponds to approximately the inverse of its k_{gp}, given that k_{gp} is held constant. We simulated partitioning under a closed system in which condensation of a species depletes its gas-phase mass concentration (C_{g}) while the particle-phase mass concentration increases (C_{p}) whereas the opposite occurs under evaporation conditions. A closed system configuration is best suited for integration into the GEOS-Chem partitioning module as partitioning occurs within a chemical time step where the gas phase is not replenished.

For the evaluation of kinetic limitations of bulk diffusion in a single particle, the characteristic mixing timescale, τ_{mix}, can be calculated as:

$$\tau_{\text{mix}} = \frac{D_{\text{p}}^2}{4\pi^2 D_{\text{b}}} \tag{13}$$

where D_{p} is particle diameter which is assumed to be 100 nm and τ_{mix} is the timescale for a diffusing molecule to diffuse and establish a uniform concentration within the particle (Li and Shiraiwa, 2019). Note that τ_{eq} is fundamentally different from τ_{mix}, as a homogeneously mixed bulk phase is not a necessary requirement to achieve gas-particle partitioning equilibrium. Additionally, while τ_{mix} is solely determined by D_{b} and particle diameter, τ_{eq} is also affected by gas diffusion, volatility and absorptive mass concentration (Li and Shiraiwa, 2019; Maclean et al., 2017; Schervish and Shiraiwa, 2023; Shiraiwa et al., 2012). Comparison of the two timescales with regards to modeling partitioning is explored in Sect. 3.1.

The box model was designed to emulate all the relevant processes used in the standard GEOS-Chem complex scheme partitioning. Temperature, $C^0(298\,\text{K})$, particle D_{b}, and initial concentrations of the gas- and particle-phase species are all prescribed for the box model simulations. A non-volatile particle-phase species is used to establish initial background aerosol C_{OA}. The volatilities of all species are temperature-corrected using Eqs. (3) and (4).

2.2 GEOS-Chem Global Model Set up

We used the global chemical transport model, GEOS-Chem (ver. 14.1.1) to simulate organic aerosols in the troposphere (Lin et al., 2024; Yantosca et al., 2023). The model system was used to simulate the atmospheric composition in the year 2020 with a horizontal grid resolution of $4° \times 5°$ and 47 vertical layers extending to about 80 km altitude (0.1 hPa) using terrain-following (sigma) coordinates near the surface. The model spin-up was six months, after which the following 12-month outputs were recorded and analyzed. The recommended timesteps for this model resolution are 10 min for transport and 20 min for chemistry. Details on the meteorology and emission inventories used are the same as in our previous study, Luu et al. (2025). Figure S1b depicts a schematic algorithm for model predictions of viscosity, bulk diffusivity, effective mass accommodation coefficient, and kinetic partitioning, as implemented into GEOS-Chem in this study.

The full chemistry mechanism with the complex SOA scheme including semi-volatile POA was applied. In this scheme, all SOA components are represented by a volatility-basis set (VBS) based on Pye et al. (2010) apart from isoprene SOA (ISOA) and organo-nitrate SOA, which are modeled through a reactive uptake scheme (Fisher et al., 2016; Marais et al., 2016). Thus, ISOA, excluded from the VBS bins, are also excluded from contributing to the absorbing SOA mass for partitioning purposes, while we do include ISOA for particle phase state calculations. D_b is calculated based on assigned glass transition temperature (T_g) values, temperature, relative humidity, and particle mass concentrations. Assigned T_g values were based on our previous study (Luu et al., 2025). Briefly, T_g of SOA component in each volatility bin ($T_{g,i}$) is calculated based on each component's volatility and oxygen-to-carbon (O : C) ratio (Table S1) (Li et al., 2020):

$$T_{g,i} = 289.10 - 16.50 \times \log_{10} C^0 - 0.29 \times \left[\left[\log_{10} C^0 \right]^2 + 3.23 \times \log_{10} C^0 \,(\mathrm{O} : \mathrm{C}) \right] \quad (14)$$

T_g of dry SOA is calculated considering mass fraction of each component and T_g of SOA at ambient RH is calculated considering water uptake using the Gordon-Taylor equation. Using the modified Vogel-Fulcher-Tammann (VFT) equation, T_g, is converted to particle viscosity, which is then converted to D_b with the fractional Stokes-Einstein equation. The detailed steps including key equations and parameters can be found in our previous studies (Li et al., 2020; Luu et al., 2025; Shiraiwa et al., 2017).

For the current work, only reversibly partitioning species are modified which includes the oxidation products of monoterpenes and sesquiterpenes (TSOA) and oxidation products of light aromatics (ASOA) and intermediate volatility organic compounds (IVOCs). The VBS for TSOA covers C^0 of 0.1, 1, 10, and 100 $\mu g\,m^{-3}$, while ASOA uses C^0 of 10^{-10} (nonvolatile), 1, 10, and 100 $\mu g\,m^{-3}$ (Yantosca et al., 2023). In addition, we updated the heat of vaporization, previously assumed as 42 kJ mol^{-1} for all organic species, to be temperature and volatility dependent using Eq. (4) (Pye et al., 2010; Pye and Seinfeld, 2010). To maintain consistency with our previous methodology, we adjusted the molecular weights of all SOA components based on molecular corridors (Shiraiwa et al., 2014), as shown in Table S1 in the Supplement.

While the aforementioned kinetic theory behind gas-particle partitioning has been applied in process-level modeling, large-scale transport models such as GEOS-Chem primarily rely on a thermodynamic partitioning method known as absorptive partitioning theory (Chung and Seinfeld, 2002). An alternative configuration for GEOS-Chem coupled with an online aerosol microphysics module (TOMAS) does not utilize thermodynamic partitioning as SOA is treated as non-volatile. GEOS-Chem-TOMAS, however, portions the total SOA mass based on the calculated effective surface area with the unity mass accommodation ($\alpha = 1$) assumption (D'Andrea et al., 2013; Pierce and Adams, 2009). The details of absorptive partitioning method solving for the equilibrium gas and particle concentration values via a root finding algorithm is further explained in Chung and Seinfeld (2002). This necessitates that chemical equilibrium is reached within the model's chemical time step (Kanakidou et al., 2005). This assumption is, however, not always true, especially when the particle phase state is highly viscous. Thus, we use α_{eff} to account for these kinetic limitations to SOA partitioning with an assumption of particle diameter of 100 nm.

The composition-dependent D_b is used to determine which algorithm the gas-particle partitioning proceeds through: (1) default GEOS-Chem instantaneous equilibrium or the (2) analytical solution as elaborated on in Sect. 3.1. If the analytical solution is selected, the condensation sink is calculated as shown in Eqs. (5), (6) using α_{eff} and Eq. (12) is used to determine final gas and particle concentrations at the end of the chemical time step.

3 Results and Discussion

We first show the box model results of six representative cases to illustrate how different partitioning treatments of the condensing species affect the time evolution of its gas-phase and particle-phase concentrations. Then we show GEOS-Chem results on the impact of the updated partitioning scheme on simulated global SOA budgets.

3.1 Zero-dimensional Box Model Simulations

Figure 1 shows six exemplary simulation results for the partitioning of a semi-volatile species of (panels a, d) $C^0 = 0.1\,\mu g\,m^{-3}$, (panels b, e) $10\,\mu g\,m^{-3,}$ or (panels c, f) $100\,\mu g\,m^{-3}$. The initial seed concentration is assumed to be $10\,\mu g\,m^{-3}$ with a number concentration of $1 \times 10^4\,cm^{-3}$, representative of polluted conditions, and the initial particle diameter is 100 nm. Initial mass concentrations of semi-volatile species in the gas and particle phases are set to 0.1 and $0\,\mu g\,m^{-3}$, respectively. Two D_b cases are tested for the particle phase: $D_b = 10^{-11}\,cm^2\,s^{-1}$ (panels a, b, c) or $10^{-18}\,cm^2\,s^{-1}$ (panels d, e, f). Per case, three simulations are shown where the treatment of partitioning differs: (1) by solving the system of ODEs numerically, Eqs. (1) and (2) with α_{eff}, (2) by solving the analytical solution, Eq. (12), or (3) same as method (1) except with the assumption of perfect mass accommodation ($\alpha = 1$). An internal time stepping loop is used to iteratively recalculate the condensation sink for both the numerical and analytical solutions.

For partitioning into liquid particles (Fig. 1a–c), particle-phase concentrations reach equilibrium concentrations rapidly with τ_{eq} of $\sim 10^2$ s, equivalent to the condensation sink timescale set by gas-phase diffusion, indicating little kinetic limitations of bulk diffusion and a well-mixed particle bulk with τ_{mix} of ~ 0.03 s. Note that τ_{eq} is longer than τ_{mix} as the partitioning is governed by gas-phase diffusion and the condensation sink rather than D_b. The numerical solutions whether using α_{eff} (black lines) or $\alpha = 1$ (red dotted lines) give identical results as α_{eff} is almost 1 with high D_b. The analytical solution (blue dashed lines) also yields practically identical results. Figure 1d–f present simulations for highly viscous particles ($D_b = 10^{-18}\,cm^2\,s^{-1}$) with τ_{mix} of $\sim 2 \times 10^6$ s, showing that partitioning proceeds with much longer equilibration timescales ($\tau_{eq} > 10^4$ s) due to strong kinetic limitations of bulk diffusion. The simulations with $\alpha = 1$ (red dotted lines) overestimates partitioning rates substantially. For the partitioning of low volatility species with $C^0 = 0.1\,\mu g\,m^{-3}$ (Fig. 1d), τ_{eq} is shorter at $\sim 10^4$ s as partitioning occurs relatively quicker compared to complete mixing. This is due to low volatility nature of the condensing species rapidly establishing a local equilibrium between the gas phase and the near-surface bulk (at the penetration depth) (Li and Shiraiwa, 2019). With higher volatility ($C^0 = 10$ and $100\,\mu g\,m^{-3}$ in Fig. 1e and f, respectively), τ_{eq} becomes longer as re-evaporation becomes relevant due to their semi-volatile nature. However, in this case τ_{mix} overestimates τ_{eq} as partitioning is finished before a well-mixed bulk is established; the use of τ_{mix} to represent partitioning timescale would lead to underestimation of SOA mass. This further exemplifies how the two timescales cannot be interchangeable as they are physically distinct. For all cases represented in Fig. 1, both the numerical and analytical solutions are identical in simulating particle growth. Overall, τ_{eq} can be longer than the CTM chemical timestep of 20 min under a multitude of ambient conditions, indicating that proper consideration of kinetic limitations of bulk diffusion is required.

To further probe the parameter space for kinetic partitioning, we computed contour plots of τ_{eq} as a function of D_b, C^0, and C_{OA} of 0.1, 1 and $10\,\mu g\,m^{-3}$. Figure 2 shows the contour plots of τ_{eq} as calculated using the numerical solution. Note that the simulations were also conducted for evaporation, yielding very similar timescales and the results of Fig. 2 are directly applicable to evaporation (Shiraiwa and Seinfeld, 2012; Shiraiwa et al., 2013). In the low bulk diffusivity ($D_b < 10^{-15}\,cm^2\,s^{-1}$) regime, τ_{eq} becomes prolonged with lower D_b due to kinetic limitations of bulk diffusion, while τ_{eq} shortens for lower C^0 as partitioning becomes largely determined by the condensation sink as there is efficient condensation with very slow re-evaporation of lower volatility compounds (Li and Shiraiwa, 2019). τ_{eq} is shorter for higher C_{OA} due to higher condensation sink, while this dependence is weaker compared to D_b and C^0. With an increased mass loading, the effect of bulk diffusivity on τ_{eq} is slightly lessened by the larger condensation sink. Figure S2 shows the contour plots of τ_{eq} calculated using the analytical solution to partitioning and reproduces very similar predicted τ_{eq} as the numerical solution in Fig. 2. Using the average case of $C_{OA} \sim 1\,\mu g\,m^{-3}$, τ_{eq} is shorter than or equal to 20 min for all C^0 when $D_b \geq 10^{-15}\,cm^2\,s^{-1}$; therefore, we can apply the instantaneous equilibrium solution for particles with little bulk diffusion limitations (demarked in green) (Fig. 3b). In this equilibrium regime, τ_{eq} exhibits sensitivity to C^0 where lower C^0 corresponds to a prolonged τ_{eq} as more mass transfer must occur to reach equilibrium conditions. In more pristine conditions where the background aerosol concentrations are lower, i.e. $C_{OA} < 1\,\mu g\,m^{-3}$, and τ_{eq} is greater than 20 min when $D_b > 10^{-15}\,cm^2\,s^{-1}$then there may be slight overestimation in the partitioned mass however this is not expected to be large as the aerosol burden in these areas would be minimal.

When particles are highly viscous with $D_b < 10^{-15}\,cm^2\,s^{-1}$, kinetic partitioning needs to be applied. The analytical solution (Fig. 2e) is an adequate representation of partitioning behavior as benchmarked by the numerical solution (Fig. 2b); thus, partitioning can be approximated by Eq. (12) where the instantaneous analytical solution can be applied at $D_b < 10^{-15}\,cm^2\,s^{-1}$. For integration into GEOS-Chem, additional internal time stepping for partitioning may be undesirable as only the partitioned mass is needed at the end of the chemical time step. Figure S2 shows a contour plot of the final ($t = 20$ min) particle-phase concentration which is calculated through two approaches: (1) the numerical and analytical solutions with internal time stepping and (2) the instantaneous analytical solution without time stepping and without iteratively recalculating C_{OA} and k_{gp}. For the three tested mass loadings, when $D_b < 10^{-15}\,cm^2\,s^{-1}$ the instantaneous analytical solution exhibits a linear trend that coincides with the linear portion of the numerical (and analytical) solution contour. Thus,

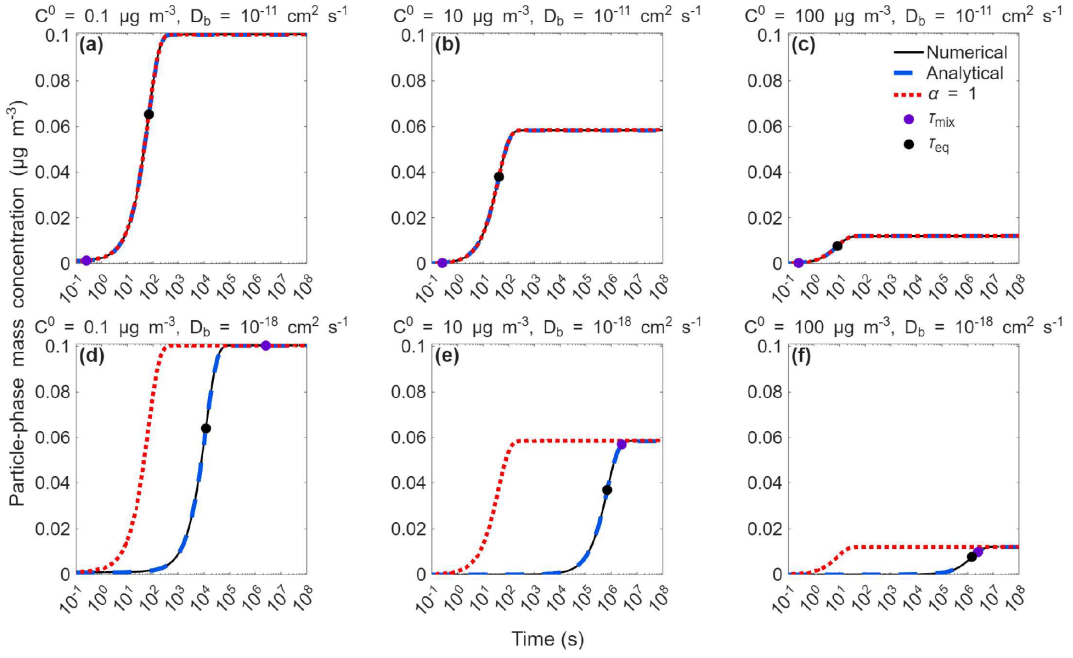

Figure 1. Temporal evolution of partitioning of semi-volatile species with $C^0 = 0.1\,\mu g\,m^{-3}$ **(a, d)**, $C^0 = 10\,\mu g\,m^{-3}$ **(b, e)**, or $C^0 = 100\,\mu g\,m^{-3}$ **(c, f)** into seed particles with initial concentrations of $10\,\mu g\,m^{-3}$ with $D_b = 10^{-11}\,cm^2\,s^{-1}$ in **(a)–(c)** or $D_b = 10^{-18}\,cm^2\,s^{-1}$ in **(d)–(f)**. The temperature was set to 298 K, and the initial particle diameter was 100 nm. τ_{mix} and τ_{eq} are marked by purple and green dots, respectively.

when $D_b < 10^{-15}\,cm^2\,s^{-1}$, the instantaneous analytical solution can be used to accurately simulate the final particle-phase (and gas-phase) concentration at 20 min.

With the assumption that the average background aerosol concentration is within the magnitude of $C_{OA} = 1\,\mu g\,m^{-3}$, we have implemented the algorithm as summarized: (1) if $D_b \geq 10^{-15}\,cm^2\,s^{-1}$, equilibrium partitioning is applied or (2) if $D_b < 10^{-15}\,cm^2\,s^{-1}$, then the instantaneous analytical solution is applied. We term this kinetic partitioning implementation as the "α_{eff} scheme" to replace the instantaneous equilibrium gas-particle partitioning scheme ("base" case) in GEOS-Chem.

3.2 Global SOA Budget Simulations

In this section, we explore the effects of kinetic partitioning on simulated global SOA budgets. We implemented the α_{eff} kinetic partitioning scheme to simulate the two sets of TSOA and ASOA species. As we have incorporated the volatility-dependent ΔH_{vap} parameterization into our methods, to accurately visualize the change due to purely partitioning scheme differences, the "base" simulation includes effects due to the change in ΔH_{vap} calculation. This is because the assumption of ΔH_{vap} in combination with the initial gas-phase concentration modulates the potential aerosol formation (or evaporation) upon cooling (heating) (Fig. S3) (Cappa and Jimenez, 2010). Lower-volatility species, e.g. $C^0 = 0.1\,\mu g\,m^{-3}$, have a higher heat of vaporization and therefore a stronger temperature dependence, such that cooling enhances their partitioning into the particle phase compared to higher-volatility compounds. Overall, the update to volatility-dependent ΔH_{vap} resulted in an increase in the global SOA burden, primarily due to enhanced partitioning and higher SOA concentrations at lower temperatures (Fig. S3).

Figure 3 presents the annually averaged D_b in SOA particles (using the α_{eff} scheme in GEOS-Chem) from the surface (vertical level 1), and two elevated hybrid-coordinate model altitudes (vertical levels 11 and 23). GEOS-Chem's hybrid sigma-pressure grid is terrain-following rather than being constant-pressure surfaces or fixed altitudes. Vertical levels 11 and 23 were selected as representative tropospheric model levels, corresponding approximately to 850 hPa (above the boundary layer) and 500 hPa (in the free troposphere), respectively, for a column at atmospheric sea level (Yantosca et al., 2023). Primarily at the surface level, SOA particles have typically $D_b \geq 10^{-10}\,cm^2\,s^{-1}$, indicating liquid-like particles with little kinetic limitations to partitioning. Western US, northern Africa, and the Tibetan Plateau are predicted to have slightly lower D_b representative of semisolid particles. Above the standard 850 hPa layer in these regions, lower D_b becomes more predominant at higher altitudes. At 500 hPa, D_b is expected to be mostly smaller than $\sim 10^{-15}\,cm^2\,s^{-1}$ in highly viscous particles apart from equatorial continents such as northern South America, sub-Saharan Africa, and Southeast Asia where SOA particles are less viscous with higher

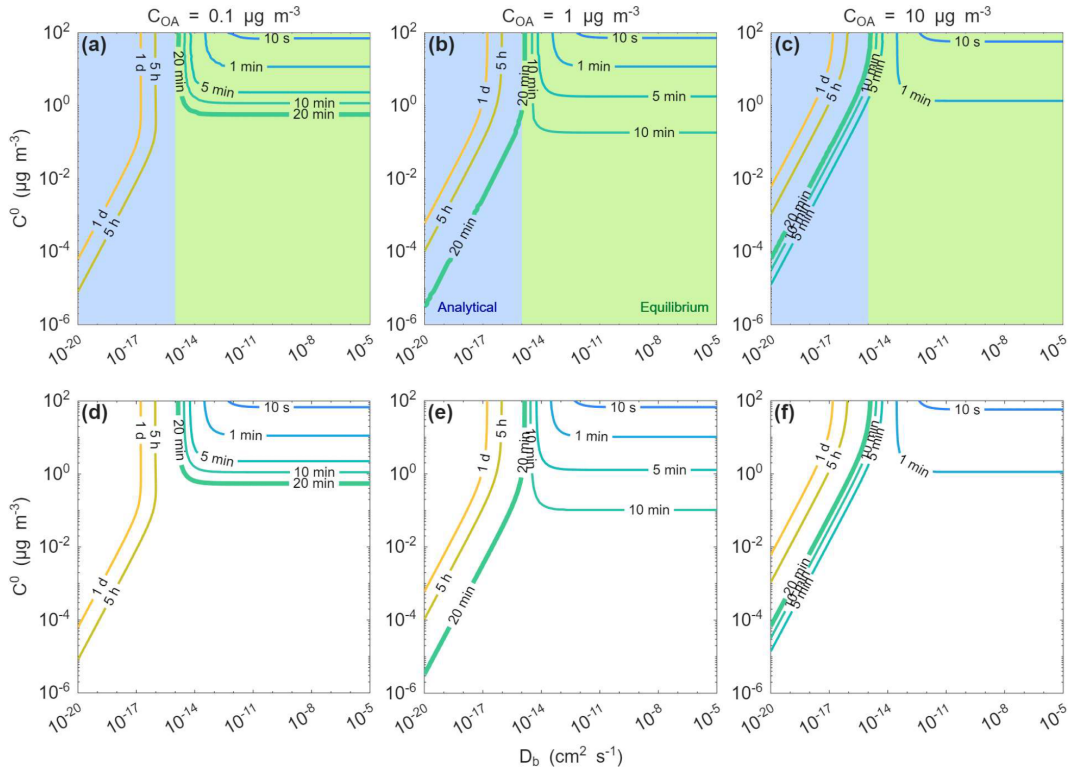

Figure 2. Contour plot of equilibration timescale (τ_{eq}) calculated using the numerical solution as a function of bulk diffusivity (D_b), saturation mass concentration (C^0), and initial pre-existing particle concentrations (C_{OA}) of **(a, d)** 0.1 μg m^{-3}, **(b, e)** 1 μg m^{-3}, and **(c, d)** 10 μg m^{-3}. The τ_{eq} is calculated using the numerical solution **(a–c)** and by the analytical solution **(d–f)**. Two colored regimes are depicted: (1) when $D_b \geq 10^{-15}$ cm^2 s^{-1}, equilibrium partitioning is applied (in green) and (2) if $D_b < 10^{-15}$ cm^2 s^{-1}, then the instantaneous analytical solution is applicable (in blue). The initial gas-phase concentration was 0.1 μg m^{-3} (to simulate condensation), or the initial particle-phase concentration was 0.1 μg m^{-3} (to simulate evaporation), and the temperature was set to 298 K.

D_b. The spatial distribution of D_b agrees well with previous phase state predictions for large-scale models (Luu et al., 2025; Shiraiwa et al., 2017).

Figure 4 shows the percent difference between annually predicted SOA budget with the α_{eff} kinetic partitioning scheme (see actual SOA mass loadings in Fig. S4) compared to the base case (Fig. S5). At the surface level, both schemes predict very similar concentrations, showing little-to-no changes in most regions. The α_{eff} scheme predicts up to 10 % less mass over the western and central US due to kinetically limited condensational growth on viscous particles (Fig. 3c). Northern Africa and Tibetan Plateau are predicted to have roughly 20 % higher SOA mass with the α_{eff} scheme due to kinetic limitations to evaporation as low C_{OA} and high temperature conditions drive net evaporation in these regions. At 850 hPa, western US is predicted to have up to 10 % less SOA mass predicted by the α_{eff} scheme, while offshore is predicted to have roughly 20 % more SOA mass. Other regions such as off the coasts of Northwestern Africa, South Africa, and Chile are also predicted to have increased SOA mass up to 40 %.

At 500 hPa, the effects of kinetic limitations on partitioning become significant, reaching upwards of 50 % greater predicted SOA mass along the equatorial and mid-latitudes as evaporation is suppressed for glassy particles. Over the remote oceans (Indian and Pacific Oceans, 10° N, 135° W and 0° N, 90° E) and central US, we predict up to an order of magnitude SOA budget increase in the upper troposphere (Figs. S4a and S5a). This occurrence may be driven by the Hadley cell in the region that lifts SOA and its precursors to the tropical tropopause, particularly in the tropical rainforest regions in the Amazon, Congo, and Oceania. These continental detainment regions are more humid than elsewhere in the tropical upper troposphere and hence have higher D_b values (Fig. 3a) allowing SOA formation in cold temperatures. As the tropical tropopause air undergoes subsidence in the Hadley cell, the temperature increases, which drives evaporation; however, the RH simultaneously decreases, which lowers D_b more than the increasing temperature increases D_b (Fig. S6). Hence, the descending regions of the Hadley cell in the subtropics have $D_b < 10^{-16}$ cm^2 s^{-1}. While the warming temperatures drive evaporation in the base simulations, the low D_b values greatly delay evaporation with the α_{eff}

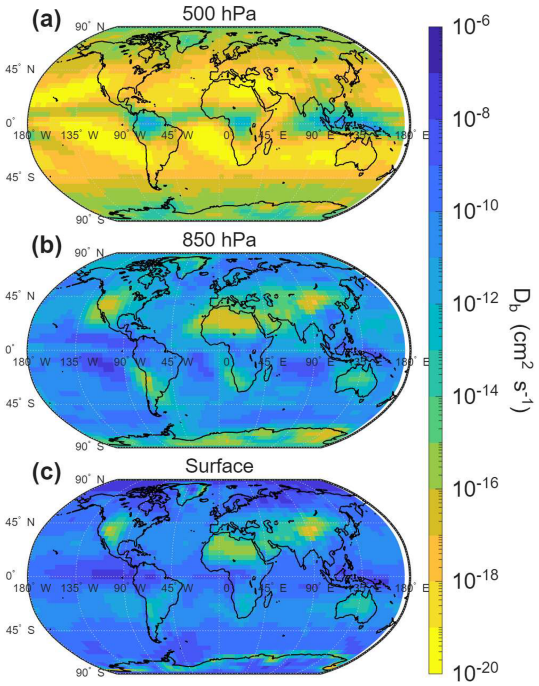

Figure 3. Simulated annually averaged bulk diffusivities (D_b) in SOA particles at selected representative tropospheric model levels which correspond to **(a)** 500 hPa and **(b)** 850 hPa for a column at atmospheric sea level. While **(c)** at the surface, corresponds to the true fixed terrain-following pressure surface.

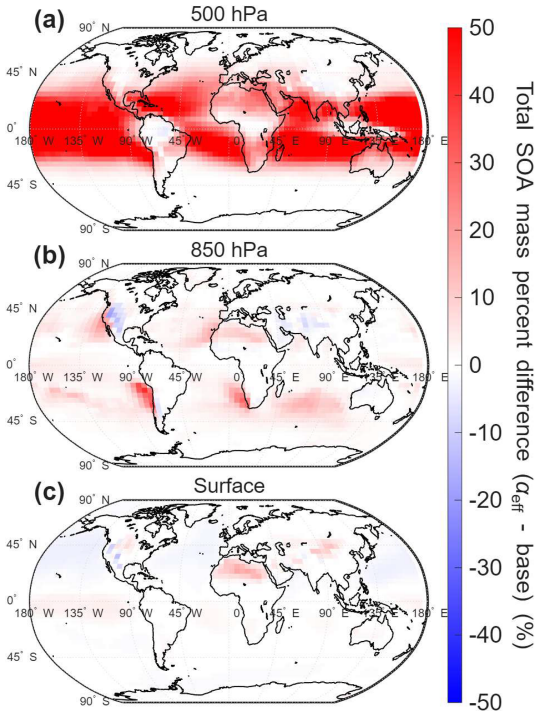

Figure 4. Predicted annual percent SOA mass loading differences **(a)** at the free troposphere, **(b)** above the boundary layer, and **(c)** at the surface between the α_{eff} kinetic and base case partitioning scheme simulations.

scheme, leading to higher concentrations in this simulation. This is expected as solid particles are more prevalent under free troposphere conditions (low average temperatures and low C_{OA}) throughout the year (Figs. 3 and S4). During each season at 500 hPa, the predicted SOA mass difference trend prevails because of kinetic limitations on evaporation when $D_b < 10^{-16}$ cm^2 s^{-1} (Fig. S7). The suppression of evaporation is more prominent for higher volatility compounds with $C^*(298\,\text{K}) = 10$ and 100 µg m^{-3} with up to 50 % higher mass predicted with the α_{eff} scheme for a majority of the mid- to equatorial latitudes (Fig. S8). The annual lower troposphere averaging approximately 1 % increase while the upper troposphere is about 15 % increase in the SOA budget (Table S2).

We show the seasonality of the SOA budget percent differences at the surface in Fig. 5. In Northern hemisphere winter, the α_{eff} kinetic partitioning scheme predicts roughly a 40 % decrease in SOA mass in the Western US but an approximately 30 % increase in Saharan Africa (Fig. 5a). As for spring, there is a mixture of an increase in predicted SOA mass in Northern Great Plains of the US extending into Canada with a small decrease for Southwestern US (Fig. 5b). There is also up to a 50 % increase in SOA budget in Saharan Africa and as much as 40 % in the Tibetan Plateau. With increased average surface temperatures in the summer months, there are virtually no differences in predicted SOA mass apart from the Tibetan Plateau as the equilibrium partitioning assumption is valid when $D_b > 10^{-15}$ cm^2 s^{-1} (Fig. S9c). The following autumn months show a mixture of enhancement and reduction in the SOA budget in western US and a slight increase across Saharan Africa, Central Asia, and the Tibetan Plateau. From these plots, we observe that each season demonstrates distinct spatial patterns of SOA budget discrepancies when kinetic limitations are applied to the partitioning scheme. It is projected that on a finer temporal resolution on the span of weeks or days, typically simulated for field campaign comparisons, weather variability may make these predicted differences more significant, yet this remains to be further investigated.

From our benchmarking, a one-month simulation has a wall time of roughly 6.6 h from the base scheme compared to the α_{eff} scheme at < 6.5 h (Table S3). The memory utilized by both schemes indicates that the α_{eff} scheme requires the same or less maximum memory usage. Truly significant differences between computational costs may slightly differ depending on run-to-run variability, however it is apparent that the α_{eff} partitioning scheme does not add any computational cost.

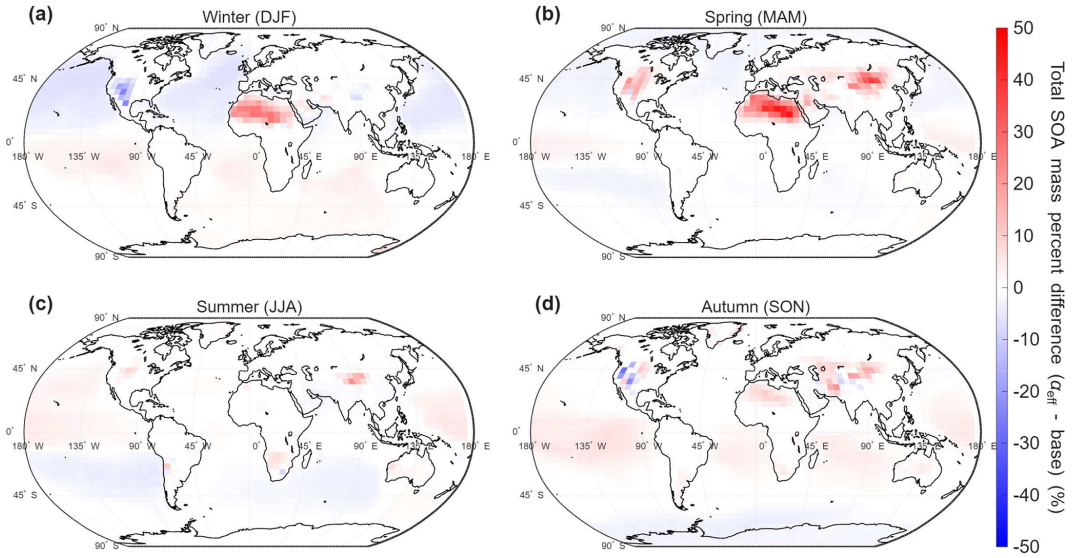

Figure 5. Predicted seasonal variations in percent SOA budget differences at the surface, during Northern hemisphere **(a)** winter (December–January–February), **(b)** spring (March–April–May), **(c)** summer (June–July–August), and **(d)** autumn (September–October–November).

4 Method Limitations and Future Needs

We address limitations in our methods and future needs. In the complex scheme, oxygenated primary organic aerosol (OPOA) is formed through OH oxidation of emitted primary organic gases (EPOG), producing oxidized primary organic gases (OPOG) that reversibly partition into OPOA (Pai et al., 2020). Therefore, previous studies aimed at quantifying simulated OA burden have categorized OPOA differently either as POA (Pai et al., 2020; Pye and Seinfeld, 2010) or SOA (Brewer et al., 2023; Murphy et al., 2014). In this study, we have chosen to omit OPOA from our main SOA phase state calculations, as only two volatility bins each are used to represent both EPOG and their oxidation products, OPOA, which may not be sufficient constraints especially for phase state predictions which have been validated for SOA (DeRieux et al., 2018; Shiraiwa et al., 2014). Both POA and OPOA are considered for total organic aerosol mass concentration (C_{OA}) as the absorbing mass for partitioning as in the base scheme. Additionally, potential phase state impact on isoprene-derived SOA (ISOA) is not resolved in the present work. ISOA is not treated as a reversibly partitioning species but treated as non-reversible reactive uptake in GEOS-Chem. Further development is needed to include kinetic limitations to the reactive uptake of ISOA.

In the current GEOS-Chem configuration, SOA particles are implicitly assumed to be externally mixed from inorganic compounds, if internally mixed, to be phase-separated, such that the predicted phase state represents only the organic phase. Consequently, the predicted viscosity and bulk diffusivity reflect the organic phase alone. This approach does not account for the influence of inorganic species, such as ammonium sulfate, ammonium nitrate, and sodium chloride on the bulk phase state. If these inorganic compounds are well-mixed with the organic phase, they may decrease viscosity by acting as plasticizers (Koop et al., 2011). If oxygenated organics and divalent inorganic ions are mixed, it might lead to an increase of viscosity by forming highly viscous gels (Richards et al., 2020). Phase separation could also occur between SOA and POA, but they are treated as ideally well-mixed as both SOA and POA are included for the total absorbing mass (C_{OA}). We partially account for phase separation in the present work through SOA phase state calculation to determine absorptive partitioning dynamics of all partitioning SOA species. However, the effect of non-ideality determining phase separation or well-mixed bulk phase on SOA partitioning should be implemented in future studies, as has been explored in several studies (Schmedding et al., 2020; Serrano Damha et al., 2025). Additionally, SOA evaporation and heterogeneous chemistry can lead to the formation of a surface crust that may hinder further evaporation (Schervish et al., 2026; Zhou et al., 2019). Such complex effects should be further explored for potential treatments in CTMs in future studies.

α_{eff} is particle size dependent as α_{eff} is inversely related to D_p, whereas we assumed $D_p = 100\,nm$ in this study. The lack of particle-size resolution in the GEOS-Chem complex scheme limits our analysis to a single particle size. However, the size tracking capabilities of GEOS-Chem-TOMAS provide an opportunity to further investigate the effects of size-dependent kinetic limitations on the SOA budget. Note that recently a size-dependent α_{eff} has been implemented in GEOS-Chem-TOMAS to portion the SOA mass accordingly across size distribution, without altering the SOA budget (O'Donnell et al., 2025). This development, though not impacting the total partitioning mass, should be included in

further advancements in implementation of kinetic partitioning in GEOS-Chem-TOMAS.

5 Conclusions

In summary, we developed a computationally efficient method to simulate SOA phase state and its impacts on kinetic partitioning utilizing the effective mass accommodation coefficient in GEOS-Chem. This method effectively accounts for the effects of gas-phase diffusion, represented by the condensation sink, as well as particle phase state and the associated kinetic limitations on partitioning. We note that τ_{mix}, which represents kinetic limitations of bulk diffusion within SOA particles, is not an accurate representation to describe SOA partitioning in aerosol modeling. A recent study by Li et al. (2026) implemented a phase-state dependent partitioning scheme using τ_{mix} as partitioning timescale in GEOS-Chem; however, the use of τ_{mix} as an equilibration timescale of SOA partitioning would lead to inaccurate representation of phase state impacts on SOA loadings, as it ignores the effects of gas diffusion, volatility, and mass loadings on the partitioning timescale, as discussed in detail in the box modeling section.

With implementation of α_{eff} kinetic partitioning scheme in GEOS-Chem, we predict that SOA particles adopt viscous semisolid and glassy phase states in arid regions below the boundary layer and is the dominant phase state in the upper troposphere. We simulate that the kinetic limitations of SOA partitioning can lead to annual SOA mass deviation up to 50 % for mid- to equatorial latitudes compared to instantaneous equilibrium partitioning above 500 hPa. Overall, we predict relatively little change in annual SOA mass at the surface and at 850 hPa, but substantial perturbations in predicted SOA mass in dry regions and in the free troposphere. We anticipate stronger deviations for finer temporal resolution simulations as we expect a reduced dilution effect on the mass difference between the α_{eff} and base case with shorter time averaging.

As POA and SOA are difficult to differentiate in field measurements, most field campaigns report total organic aerosol (OA) mass concentration making OA model-measurement comparisons more common; typically, OA (including OPOA) mass concentrations were underpredicted at remote free tropospheric altitudes, but in some cases, OA has been overestimated (Heald et al., 2011; Hodzic et al., 2020; Pai et al., 2020). The development of the α_{eff} kinetic partitioning scheme enables comparison with aircraft observations to quantify impacts of SOA phase state in future studies. Observations of SOA mass loading in the upper troposphere would be especially compelling to investigate as predictions of high-altitude new particle formation may be improved from implementing the α_{eff} scheme for SOA partitioning. Addressing this well-known knowledge gap may help achieve closure between SOA model simulations and field observations.

Code and data availability. The GEOS-Chem model is maintained by the Harvard Atmospheric Chemistry Modelling Group and the specific version (ver. 14.1.1) used in this work is permanently archived at https://doi.org/10.5281/zenodo.7696632 (Yantosca et al., 2023). The modified carbon_mod.f90 used in this work and the 0-D box model are archived at https://doi.org/10.5281/zenodo.22099483 (Luu et al., 2026). GEOS-Chem simulation outputs are available by contacting the corresponding author.

Supplement. The supplement related to this article is available online at https://doi.org/10.5194/gmd-19-11405-2026-supplement.

Author contributions. RL, MSc, JP and MSh designed the research. RL developed the box model, GEOS-Chem implementation, and ran the simulations. RL and MSc conducted data analysis and all authors were involved in discussions. RL drafted the manuscript, MSh edited the manuscript, and all authors reviewed and commented on the paper.

Competing interests. The contact author has declared that none of the authors has any competing interests.

Disclaimer. Publisher's note: Copernicus Publications remains neutral with regard to jurisdictional claims made in the text, published maps, institutional affiliations, or any other geographical representation in this paper. The authors bear the ultimate responsibility for providing appropriate place names. Views expressed in the text are those of the authors and do not necessarily reflect the views of the publisher.

Acknowledgements. This work was funded by the U.S. National Science Foundation (AGS-2246502).

Financial support. This research has been supported by the National Science Foundation, Directorate for Geosciences (grant no. AGS-2246502).

Review statement. This paper was edited by Rolf Sander and reviewed by two anonymous referees.

References

Brewer, J. F., Jacob, D. J., Jathar, S. H., He, Y., Akherati, A., Zhai, S., Jo, D. S., Hodzic, A., Nault, B. A., Campuzano-Jost, P., Jimenez, J. L., Park, R. J., Oak, Y. J., and Liao, H.: A Scheme for Representing Aromatic Secondary Organic Aerosols in Chemical Transport Models: Application to Source Attribution of Organic Aerosols Over South Korea During the KORUS-AQ Campaign, J. Geophys. Res.-Atmos., 128, e2022JD037257, https://doi.org/10.1029/2022JD037257, 2023.

Cappa, C. D. and Jimenez, J. L.: Quantitative estimates of the volatility of ambient organic aerosol, Atmos. Chem. Phys., 10, 5409–5424, https://doi.org/10.5194/acp-10-5409-2010, 2010.

Chung, S. H. and Seinfeld, J. H.: Global distribution and climate forcing of carbonaceous aerosols, J. Geophys. Res.-Atmos., 107, https://doi.org/10.1029/2001jd001397, 2002.

D'Andrea, S. D., Häkkinen, S. A. K., Westervelt, D. M., Kuang, C., Levin, E. J. T., Kanawade, V. P., Leaitch, W. R., Spracklen, D. V., Riipinen, I., and Pierce, J. R.: Understanding global secondary organic aerosol amount and size-resolved condensational behavior, Atmos. Chem. Phys., 13, 11519–11534, https://doi.org/10.5194/acp-13-11519-2013, 2013.

DeRieux, W.-S. W., Li, Y., Lin, P., Laskin, J., Laskin, A., Bertram, A. K., Nizkorodov, S. A., and Shiraiwa, M.: Predicting the glass transition temperature and viscosity of secondary organic material using molecular composition, Atmos. Chem. Phys., 18, 6331–6351, https://doi.org/10.5194/acp-18-6331-2018, 2018.

Fisher, J. A., Jacob, D. J., Travis, K. R., Kim, P. S., Marais, E. A., Chan Miller, C., Yu, K., Zhu, L., Yantosca, R. M., Sulprizio, M. P., Mao, J., Wennberg, P. O., Crounse, J. D., Teng, A. P., Nguyen, T. B., St. Clair, J. M., Cohen, R. C., Romer, P., Nault, B. A., Wooldridge, P. J., Jimenez, J. L., Campuzano-Jost, P., Day, D. A., Hu, W., Shepson, P. B., Xiong, F., Blake, D. R., Goldstein, A. H., Misztal, P. K., Hanisco, T. F., Wolfe, G. M., Ryerson, T. B., Wisthaler, A., and Mikoviny, T.: Organic nitrate chemistry and its implications for nitrogen budgets in an isoprene- and monoterpene-rich atmosphere: constraints from aircraft (SEAC^{4}RS) and ground-based (SOAS) observations in the Southeast US, Atmos. Chem. Phys., 16, 5969–5991, https://doi.org/10.5194/acp-16-5969-2016, 2016.

Hallquist, M., Wenger, J. C., Baltensperger, U., Rudich, Y., Simpson, D., Claeys, M., Dommen, J., Donahue, N. M., George, C., Goldstein, A. H., Hamilton, J. F., Herrmann, H., Hoffmann, T., Iinuma, Y., Jang, M., Jenkin, M. E., Jimenez, J. L., Kiendler-Scharr, A., Maenhaut, W., McFiggans, G., Mentel, Th. F., Monod, A., Prévôt, A. S. H., Seinfeld, J. H., Surratt, J. D., Szmigielski, R., and Wildt, J.: The formation, properties and impact of secondary organic aerosol: current and emerging issues, Atmos. Chem. Phys., 9, 5155–5236, https://doi.org/10.5194/acp-9-5155-2009, 2009.

He, Y., Bilsback, K. R., Shrivastava, M., Zaveri, R. A., Shilling, J. E., Seinfeld, J. H., Zhao, B., Wang, S., Cappa, C. D., Pierce, J. R., and Jathar, S. H.: Kinetic Modeling of Secondary Organic Aerosol in a Weather-Chemistry Model: Parameterizations, Processes, and Predictions for GOAmazon, ACS ES&T Air, 2, 249–263, https://doi.org/10.1021/acsestair.4c00240, 2025.

Heald, C. L., Coe, H., Jimenez, J. L., Weber, R. J., Bahreini, R., Middlebrook, A. M., Russell, L. M., Jolleys, M., Fu, T.-M., Allan, J. D., Bower, K. N., Capes, G., Crosier, J., Morgan, W. T., Robinson, N. H., Williams, P. I., Cubison, M. J., DeCarlo, P. F., and Dunlea, E. J.: Exploring the vertical profile of atmospheric organic aerosol: comparing 17 aircraft field campaigns with a global model, Atmos. Chem. Phys., 11, 12673–12696, https://doi.org/10.5194/acp-11-12673-2011, 2011.

Hindmarsh, A. C.: ODEPACK, A Systematized Collection of ODE Solvers, Sci. Comput., 1, 55–64, 1983.

Hodzic, A., Kasibhatla, P. S., Jo, D. S., Cappa, C. D., Jimenez, J. L., Madronich, S., and Park, R. J.: Rethinking the global secondary organic aerosol (SOA) budget: stronger production, faster removal, shorter lifetime, Atmos. Chem. Phys., 16, 7917–7941, https://doi.org/10.5194/acp-16-7917-2016, 2016.

Hodzic, A., Campuzano-Jost, P., Bian, H., Chin, M., Colarco, P. R., Day, D. A., Froyd, K. D., Heinold, B., Jo, D. S., Katich, J. M., Kodros, J. K., Nault, B. A., Pierce, J. R., Ray, E., Schacht, J., Schill, G. P., Schroder, J. C., Schwarz, J. P., Sueper, D. T., Tegen, I., Tilmes, S., Tsigaridis, K., Yu, P., and Jimenez, J. L.: Characterization of organic aerosol across the global remote troposphere: a comparison of ATom measurements and global chemistry models, Atmos. Chem. Phys., 20, 4607–4635, https://doi.org/10.5194/acp-20-4607-2020, 2020.

Jensen, L. N., Kristensen, K., Iversen, E. M., Canagaratna, M. R., Roldin, P., and Bilde, M.: Nature of Temperature-Induced Phase Transitions in Secondary Organic Aerosol Particles, Environ. Sci. Technol., 59, 24359–24367, https://doi.org/10.1021/acs.est.5c08582, 2025.

Jimenez, J. L., Canagaratna, M. R., Donahue, N. M., Prevot, A. S. H., Zhang, Q., Kroll, J. H., DeCarlo, P. F., Allan, J. D., Coe, H., Ng, N. L., Aiken, A. C., Docherty, K. S., Ulbrich, I. M., Grieshop, A. P., Robinson, A. L., Duplissy, J., Smith, J. D., Wilson, K. R., Lanz, V. A., Hueglin, C., Sun, Y. L., Tian, J., Laaksonen, A., Raatikainen, T., Rautiainen, J., Vaattovaara, P., Ehn, M., Kulmala, M., Tomlinson, J. M., Collins, D. R., Cubison, M. J., E., Dunlea, J., Huffman, J. A., Onasch, T. B., Alfarra, M. R., Williams, P. I., Bower, K., Kondo, Y., Schneider, J., Drewnick, F., Borrmann, S., Weimer, S., Demerjian, K., Salcedo, D., Cottrell, L., Griffin, R., Takami, A., Miyoshi, T., Hatakeyama, S., Shimono, A., Sun, J. Y., Zhang, Y. M., Dzepina, K., Kimmel, J. R., Sueper, D., Jayne, J. T., Herndon, S. C., Trimborn, A. M., Williams, L. R., Wood, E. C., Middlebrook, A. M., Kolb, C. E., Baltensperger, U., and Worsnop, D. R.: Evolution of Organic Aerosols in the Atmosphere, Science, 326, 1525–1529, https://doi.org/10.1126/science.1180353, 2009.

Julin, J., Winkler, P. M., Donahue, N. M., Wagner, P. E., and Riipinen, I.: Near-Unity Mass Accommodation Coefficient of Organic Molecules of Varying Structure, Environ. Sci. Technol., 48, 12083–12089, https://doi.org/10.1021/es501816h, 2014.

Kanakidou, M., Seinfeld, J. H., Pandis, S. N., Barnes, I., Dentener, F. J., Facchini, M. C., Van Dingenen, R., Ervens, B., Nenes, A., Nielsen, C. J., Swietlicki, E., Putaud, J. P., Balkanski, Y., Fuzzi, S., Horth, J., Moortgat, G. K., Winterhalter, R., Myhre, C. E. L., Tsigaridis, K., Vignati, E., Stephanou, E. G., and Wilson, J.: Organic aerosol and global climate modelling: a review, Atmos. Chem. Phys., 5, 1053–1123, https://doi.org/10.5194/acp-5-1053-2005, 2005.

Kirkby, J., Amorim, A., Baltensperger, U., Carslaw, K. S., Christoudias, T., Curtius, J., Donahue, N. M., Haddad, I. E., Flagan, R. C., Gordon, H., Hansel, A., Harder, H., Junninen, H., Kulmala, M., Kürten, A., Laaksonen, A., Lehtipalo, K., Lelieveld, J., Möhler, O., Riipinen, I., Stratmann, F., Tomé, A., Virtanen, A.,

Volkamer, R., Winkler, P. M., and Worsnop, D. R.: Atmospheric new particle formation from the CERN CLOUD experiment, Nat. Geosci., 16, 948–957, https://doi.org/10.1038/s41561-023-01305-0, 2023.

Koop, T., Bookhold, J., Shiraiwa, M., and Pöschl, U.: Glass transition and phase state of organic compounds: dependency on molecular properties and implications for secondary organic aerosols in the atmosphere, Phys. Chem. Chem. Phys., 13, 19238–19255, https://doi.org/10.1039/C1CP22617G, 2011.

Kroll, J. H. and Seinfeld, J. H.: Chemistry of secondary organic aerosol: Formation and evolution of low-volatility organics in the atmosphere, Atmos. Environ., 42, 3593–3624, https://doi.org/10.1016/j.atmosenv.2008.01.003, 2008.

Kuwata, M., Zorn, S. R., and Martin, S. T.: Using elemental ratios to predict the density of organic material composed of carbon, hydrogen, and oxygen, Environ. Sci. Technol., 46, 787–794, https://doi.org/10.1021/es202525q, 2012.

Li, Y. and Shiraiwa, M.: Timescales of secondary organic aerosols to reach equilibrium at various temperatures and relative humidities, Atmos. Chem. Phys., 19, 5959–5971, https://doi.org/10.5194/acp-19-5959-2019, 2019.

Li, Y., Day, D. A., Stark, H., Jimenez, J. L., and Shiraiwa, M.: Predictions of the glass transition temperature and viscosity of organic aerosols from volatility distributions, Atmos. Chem. Phys., 20, 8103–8122, https://doi.org/10.5194/acp-20-8103-2020, 2020.

Li, Y., Heald, C. L., Miao, R., Campuzano-Jost, P., and Jimenez, J. L.: Global Impacts of Simulating Organic Aerosol Phase State, Environ. Sci. Technol., https://doi.org/10.1021/acs.est.5c13238, 2026.

Lin, H., Emmons, L. K., Lundgren, E. W., Yang, L. H., Feng, X., Dang, R., Zhai, S., Tang, Y., Kelp, M. M., Colombi, N. K., Eastham, S. D., Fritz, T. M., and Jacob, D. J.: Intercomparison of GEOS-Chem and CAM-chem tropospheric oxidant chemistry within the Community Earth System Model version 2 (CESM2), Atmos. Chem. Phys., 24, 8607–8624, https://doi.org/10.5194/acp-24-8607-2024, 2024.

Liu, X., Day, D. A., Krechmer, J. E., Brown, W., Peng, Z., Ziemann, P. J., and Jimenez, J. L.: Direct measurements of semi-volatile organic compound dynamics show near-unity mass accommodation coefficients for diverse aerosols, Commun. Chem., 2, 98, https://doi.org/10.1038/s42004-019-0200-x, 2019.

Luu, R., Schervish, M., June, N. A., O'Donnell, S. E., Jathar, S. H., Pierce, J. R., and Shiraiwa, M.: Global Simulations of Phase State and Equilibration Time Scales of Secondary Organic Aerosols with GEOS-Chem, ACS Earth Space Chem., 9, 288–302, https://doi.org/10.1021/acsearthspacechem.4c00281, 2025.

Luu, R., Schervish, M., O'Donnell, E. S., Pierce, R. J., and Shiraiwa, M.: carbon_mod – added aeff kinetic partitioning scheme, In (Version v1.0.0-alpha), Zenodo [code, data set], https://doi.org/10.5281/zenodo.22099483, 2026.

Maclean, A. M., Butenhoff, C. L., Grayson, J. W., Barsanti, K., Jimenez, J. L., and Bertram, A. K.: Mixing times of organic molecules within secondary organic aerosol particles: a global planetary boundary layer perspective, Atmos. Chem. Phys., 17, 13037–13048, https://doi.org/10.5194/acp-17-13037-2017, 2017.

Marais, E. A., Jacob, D. J., Jimenez, J. L., Campuzano-Jost, P., Day, D. A., Hu, W., Krechmer, J., Zhu, L., Kim, P. S., Miller, C. C., Fisher, J. A., Travis, K., Yu, K., Hanisco, T. F., Wolfe, G. M., Arkinson, H. L., Pye, H. O. T., Froyd, K. D., Liao, J., and McNeill, V. F.: Aqueous-phase mechanism for secondary organic aerosol formation from isoprene: application to the southeast United States and co-benefit of SO2 emission controls, Atmos. Chem. Phys., 16, 1603–1618, https://doi.org/10.5194/acp-16-1603-2016, 2016.

Murphy, B. N., Donahue, N. M., Robinson, A. L., and Pandis, S. N.: A naming convention for atmospheric organic aerosol, Atmos. Chem. Phys., 14, 5825–5839, https://doi.org/10.5194/acp-14-5825-2014, 2014.

O'Brien, R. E., Neu, A., Epstein, S. A., MacMillan, A. C., Wang, B., Kelly, S. T., Nizkorodov, S. A., Laskin, A., Moffet, R. C., and Gilles, M. K.: Physical properties of ambient and laboratory-generated secondary organic aerosol, Geophys. Res. Lett., 41, 4347–4353, https://doi.org/10.1002/2014GL060219, 2014.

O'Donnell, S. E., Croft, B., Ford, B., June, N. A., Kuang, C., Singh, A., Chang, R. Y.-W., Collins, D. R., Hakala, S., Jathar, S. H., Paasonen, P., Shrivastava, M., Smith, J. N., and Pierce, J. R.: Going Off Grid: A Comparative Study of the Lagrangian and Eulerian Perspectives of New Particle Formation Events, J. Geophys. Res.-Atmos., 130, e2025JD043713, https://doi.org/10.1029/2025JD043713, 2025.

Pai, S. J., Heald, C. L., Pierce, J. R., Farina, S. C., Marais, E. A., Jimenez, J. L., Campuzano-Jost, P., Nault, B. A., Middlebrook, A. M., Coe, H., Shilling, J. E., Bahreini, R., Dingle, J. H., and Vu, K.: An evaluation of global organic aerosol schemes using airborne observations, Atmos. Chem. Phys., 20, 2637–2665, https://doi.org/10.5194/acp-20-2637-2020, 2020.

Pankow, J. F.: An absorption model of gas/particle partitioning of organic compounds in the atmosphere, Atmos. Environ., 28, 185–188, https://doi.org/10.1016/1352-2310(94)90093-0, 1994.

Pankow, J. F.: Gas/particle partitioning of neutral and ionizing compounds to single and multi-phase aerosol particles. 1. Unified modeling framework, Atmos. Environ., 37, 3323–3333, https://doi.org/10.1016/S1352-2310(03)00346-7, 2003.

Pierce, J. R. and Adams, P. J.: Uncertainty in global CCN concentrations from uncertain aerosol nucleation and primary emission rates, Atmos. Chem. Phys., 9, 1339–1356, https://doi.org/10.5194/acp-9-1339-2009, 2009.

Pöschl, U. and Shiraiwa, M.: Multiphase Chemistry at the Atmosphere–Biosphere Interface Influencing Climate and Public Health in the Anthropocene, Chem. Rev., 115, 4440–4475, https://doi.org/10.1021/cr500487s, 2015.

Pöschl, U., Rudich, Y., and Ammann, M.: Kinetic model framework for aerosol and cloud surface chemistry and gas-particle interactions – Part 1: General equations, parameters, and terminology, Atmos. Chem. Phys., 7, 5989–6023, https://doi.org/10.5194/acp-7-5989-2007, 2007.

Pye, H. O. T. and Seinfeld, J. H.: A global perspective on aerosol from low-volatility organic compounds, Atmos. Chem. Phys., 10, 4377–4401, https://doi.org/10.5194/acp-10-4377-2010, 2010.

Pye, H. O. T., Chan, A. W. H., Barkley, M. P., and Seinfeld, J. H.: Global modeling of organic aerosol: the importance of reactive nitrogen (NO_x and NO_3), Atmos. Chem. Phys., 10, 11261–11276, https://doi.org/10.5194/acp-10-11261-2010, 2010.

Reid, J. P., Bertram, A. K., Topping, D. O., Laskin, A., Martin, S. T., Petters, M. D., Pope, F. D., and Rovelli, G.: The viscosity

of atmospherically relevant organic particles, Nat. Commun., 9, 956, https://doi.org/10.1038/s41467-018-03027-z, 2018.

Richards, D. S., Trobaugh, K. L., Hajek-Herrera, J., Price, C. L., Sheldon, C. S., Davies, J. F., and Davis, R. D.: Ion-molecule interactions enable unexpected phase transitions in organic-inorganic aerosol, Sci. Adv., 6, eabb5643, https://doi.org/10.1126/sciadv.abb5643, 2020.

Robinson, A. L., Donahue, N. M., Shrivastava, M. K., Weitkamp, E. A., Sage, A. M., Grieshop, A. P., Lane, T. E., Pierce, J. R., and Pandis, S. N.: Rethinking organic aerosols: Semivolatile emissions and photochemical aging, Science, 315, 1259–1262, https://doi.org/10.1126/science.1133061, 2007.

Saukko, E., Lambe, A. T., Massoli, P., Koop, T., Wright, J. P., Croasdale, D. R., Pedernera, D. A., Onasch, T. B., Laaksonen, A., Davidovits, P., Worsnop, D. R., and Virtanen, A.: Humidity-dependent phase state of SOA particles from biogenic and anthropogenic precursors, Atmos. Chem. Phys., 12, 7517–7529, https://doi.org/10.5194/acp-12-7517-2012, 2012.

Schervish, M., Donahue, N. M., and Shiraiwa, M.: Effects of volatility, viscosity, and non-ideality on particle–particle mixing timescales of secondary organic aerosols, Aerosol Sci. Tech., 58, 411–426, https://doi.org/10.1080/02786826.2023.2256827, 2024.

Schervish, M. and Shiraiwa, M.: Impact of phase state and non-ideal mixing on equilibration timescales of secondary organic aerosol partitioning, Atmos. Chem. Phys., 23, 221–233, https://doi.org/10.5194/acp-23-221-2023, 2023.

Schervish, M., Kang, H. G., Wingen, L. M., Nguyen, K., Begay, C., Wilson, J., Shrivastava, M., Chen, Y., Shilling, J. E., Ng, N. L., Pöschl, U., Berkemeier, T., Zelenyuk, A., and Shiraiwa, M.: Surface Crust Formation Controls Evaporation Kinetics of Secondary Organic Aerosols, Environ. Sci. Technol., 60, 7995–8006, https://doi.org/10.1021/acs.est.5c11018, 2026.

Schmedding, R., Rasool, Q. Z., Zhang, Y., Pye, H. O. T., Zhang, H., Chen, Y., Surratt, J. D., Lopez-Hilfiker, F. D., Thornton, J. A., Goldstein, A. H., and Vizuete, W.: Predicting secondary organic aerosol phase state and viscosity and its effect on multiphase chemistry in a regional-scale air quality model, Atmos. Chem. Phys., 20, 8201–8225, https://doi.org/10.5194/acp-20-8201-2020, 2020.

Serrano Damha, C., Gorkowski, K., and Zuend, A.: Implications of reduced-complexity aerosol thermodynamics on organic aerosol mass concentration and composition over North America, Atmos. Chem. Phys., 25, 5773–5792, https://doi.org/10.5194/acp-25-5773-2025, 2025.

Shiraiwa, M. and Pöschl, U.: Mass accommodation and gas–particle partitioning in secondary organic aerosols: dependence on diffusivity, volatility, particle-phase reactions, and penetration depth, Atmos. Chem. Phys., 21, 1565–1580, https://doi.org/10.5194/acp-21-1565-2021, 2021.

Shiraiwa, M. and Seinfeld, J. H.: Equilibration timescale of atmospheric secondary organic aerosol partitioning, Geophys. Res. Lett., 39, L24801, https://doi.org/10.1029/2012GL054008, 2012.

Shiraiwa, M., Pfrang, C., Koop, T., and Pöschl, U.: Kinetic multilayer model of gas-particle interactions in aerosols and clouds (KM-GAP): linking condensation, evaporation and chemical reactions of organics, oxidants and water, Atmos. Chem. Phys., 12, 2777–2794, https://doi.org/10.5194/acp-12-2777-2012, 2012.

Shiraiwa, M., Zuend, A., Bertram, A. K., and Seinfeld, J. H.: Gas-particle partitioning of atmospheric aerosols: interplay of physical state, non-ideal mixing and morphology, Phys. Chem. Chem. Phys., 15, 11441–11453, https://doi.org/10.1039/C3CP51595H, 2013.

Shiraiwa, M., Berkemeier, T., Schilling-Fahnestock, K. A., Seinfeld, J. H., and Pöschl, U.: Molecular corridors and kinetic regimes in the multiphase chemical evolution of secondary organic aerosol, Atmos. Chem. Phys., 14, 8323–8341, https://doi.org/10.5194/acp-14-8323-2014, 2014.

Shiraiwa, M., Li, Y., Tsimpidi, A. P., Karydis, V. A., Berkemeier, T., Pandis, S. N., Lelieveld, J., Koop, T., and Pöschl, U.: Global distribution of particle phase state in atmospheric secondary organic aerosols, Nat. Commun., 8, 15002, https://doi.org/10.1038/ncomms15002, 2017.

Shrivastava, M., Cappa, C. D., Fan, J., Goldstein, A. H., Guenther, A. B., Jimenez, J. L., Kuang, C., Laskin, A., Martin, S. T., Ng, N. L., Petaja, T., Pierce, J. R., Rasch, P. J., Roldin, P., Seinfeld, J. H., Shilling, J., Smith, J. N., Thornton, J. A., Volkamer, R., Wang, J., Worsnop, D. R., Zaveri, R. A., Zelenyuk, A., and Zhang, Q.: Recent advances in understanding secondary organic aerosol: Implications for global climate forcing, Rev. Geophys., 55, 509–559, https://doi.org/10.1002/2016RG000540, 2017.

Shrivastava, M., Fan, J., Zhang, Y., Rasool, Q. Z., Zhao, B., Shen, J., Pierce, J. R., Jathar, S. H., Akherati, A., Zhang, J., Zaveri, R. A., Gaudet, B., Liu, Y., Andreae, M. O., Pöhlker, M. L., Donahue, N. M., Wang, Y., and Seinfeld, J. H.: Intense formation of secondary ultrafine particles from Amazonian vegetation fires and their invigoration of deep clouds and precipitation, One Earth, 7, 1029–1043, https://doi.org/10.1016/j.oneear.2024.05.015, 2024.

Stolzenburg, D., Fischer, L., Vogel, A. L., Heinritzi, M., Schervish, M., Simon, M., Wagner, A. C., Dada, L., Ahonen, L. R., Amorim, A., Baccarini, A., Bauer, P. S., Baumgartner, B., Bergen, A., Bianchi, F., Breitenlechner, M., Brilke, S., Buenrostro Mazon, S., Chen, D., Dias, A., Draper, D. C., Duplissy, J., El Haddad, I., Finkenzeller, H., Frege, C., Fuchs, C., Garmash, O., Gordon, H., He, X., Helm, J., Hofbauer, V., Hoyle, C. R., Kim, C., Kirkby, J., Kontkanen, J., Kürten, A., Lampilahti, J., Lawler, M., Lehtipalo, K., Leiminger, M., Mai, H., Mathot, S., Mentler, B., Molteni, U., Nie, W., Nieminen, T., Nowak, J. B., Ojdanic, A., Onnela, A., Passananti, M., Petäjä, T., Quéléver, L. L. J., Rissanen, M. P., Sarnela, N., Schallhart, S., Tauber, C., Tomé, A., Wagner, R., Wang, M., Weitz, L., Wimmer, D., Xiao, M., Yan, C., Ye, P., Zha, Q., Baltensperger, U., Curtius, J., Dommen, J., Flagan, R. C., Kulmala, M., Smith, J. N., Worsnop, D. R., Hansel, A., Donahue, N. M., and Winkler, P. M.: Rapid growth of organic aerosol nanoparticles over a wide tropospheric temperature range, P. Natl. Acad. Sci., 115, 9122–9127, https://doi.org/10.1073/pnas.1807604115, 2018.

Stolzenburg, D., Wang, M., Schervish, M., and Donahue, N. M.: Tutorial: Dynamic organic growth modeling with a volatility basis set, J. Aerosol Sci., 166, 106063, https://doi.org/10.1016/j.jaerosci.2022.106063, 2022.

Trump, E. R., Riipinen, I., and Donahue, N. M.: Interactions between atmospheric ultrafine particles and secondary organic aerosol mass: a model study, Boreal Environ. Res., 19, https://doi.org/10.60910/wkqn-gtbz, 2014.

Tsigaridis, K., Daskalakis, N., Kanakidou, M., Adams, P. J., Artaxo, P., Bahadur, R., Balkanski, Y., Bauer, S. E., Bellouin, N.,

Benedetti, A., Bergman, T., Berntsen, T. K., Beukes, J. P., Bian, H., Carslaw, K. S., Chin, M., Curci, G., Diehl, T., Easter, R. C., Ghan, S. J., Gong, S. L., Hodzic, A., Hoyle, C. R., Iversen, T., Jathar, S., Jimenez, J. L., Kaiser, J. W., Kirkevåg, A., Koch, D., Kokkola, H., Lee, Y. H., Lin, G., Liu, X., Luo, G., Ma, X., Mann, G. W., Mihalopoulos, N., Morcrette, J.-J., Müller, J.-F., Myhre, G., Myriokefalitakis, S., Ng, N. L., O'Donnell, D., Penner, J. E., Pozzoli, L., Pringle, K. J., Russell, L. M., Schulz, M., Sciare, J., Seland, Ø., Shindell, D. T., Sillman, S., Skeie, R. B., Spracklen, D., Stavrakou, T., Steenrod, S. D., Takemura, T., Tiitta, P., Tilmes, S., Tost, H., van Noije, T., van Zyl, P. G., von Salzen, K., Yu, F., Wang, Z., Wang, Z., Zaveri, R. A., Zhang, H., Zhang, K., Zhang, Q., and Zhang, X.: The AeroCom evaluation and intercomparison of organic aerosol in global models, Atmos. Chem. Phys., 14, 10845–10895, https://doi.org/10.5194/acp-14-10845-2014, 2014.

Vaden, T. D., Imre, D., Beránek, J., Shrivastava, M., and Zelenyuk, A.: Evaporation kinetics and phase of laboratory and ambient secondary organic aerosol, P. Natl. Acad. Sci., 108, 2190–2195, https://doi.org/10.1073/pnas.1013391108, 2011.

Virtanen, A., Joutsensaari, J., Koop, T., Kannosto, J., Yli-Pirilä, P., Leskinen, J., Mäkelä, J. M., Holopainen, J. K., Pöschl, U., Kulmala, M., Worsnop, D. R., and Laaksonen, A.: An amorphous solid state of biogenic secondary organic aerosol particles, Nature, 467, 824–827, https://doi.org/10.1038/nature09455, 2010.

Yantosca, B., Sulprizio, M., Lundgren, L., kelvinhb, Keller, C., Fritz, T., 22degrees, Ridley, D., Lin, H., Bindle, L., michael-slong, Eastham, S. D., tsherwen, Downs, W., Fisher, J., Thackray, C., Holmes, C., GanLuo, Zhuang, J., Murray, L., SpaceMouse, laestrada, Shutter, J., noelleselin, Long, M., Chen, X., emily-ramnarine, gianga, Haskins, J., and Jourdan-He: geoschem/geos-chem: GEOS-Chem 14.1.1, Version 14.1.1, Zenodo [code, data set], https://doi.org/10.5281/zenodo.7696632, 2023.

Zaveri, R. A., Easter, R. C., Shilling, J. E., and Seinfeld, J. H.: Modeling kinetic partitioning of secondary organic aerosol and size distribution dynamics: representing effects of volatility, phase state, and particle-phase reaction, Atmos. Chem. Phys., 14, 5153–5181, https://doi.org/10.5194/acp-14-5153-2014, 2014.

Zhang, Z., Li, Y., Ran, H., An, J., Qu, Y., Zhou, W., Xu, W., Hu, W., Xie, H., Wang, Z., Sun, Y., and Shiraiwa, M.: Simulated phase state and viscosity of secondary organic aerosols over China, Atmos. Chem. Phys., 24, 4809–4826, https://doi.org/10.5194/acp-24-4809-2024, 2024.

Zhou, S., Hwang, B. C. H., Lakey, P. S. J., Zuend, A., Abbatt, J. P. D., and Shiraiwa, M.: Multiphase reactivity of polycyclic aromatic hydrocarbons is driven by phase separation and diffusion limitations, P. Natl. Acad. Sci., 116, 11658–11663, https://doi.org/10.1073/pnas.1902517116, 2019.

Ziemann, P. J. and Atkinson, R.: Kinetics, products, and mechanisms of secondary organic aerosol formation, Chem. Soc. Rev., 41, 6582–6605, https://doi.org/10.1039/c2cs35122f, 2012.